Interactions of Lysozyme in Concentrated Electrolyte Solutions from Dynamic Light-Scattering Measurements

Daniel E. Kuehner,* Christiane Heyer,# Christian Rämsch,# Ursula M. Fornefeld,# Harvey W. Blanch,# and John M. Prausnitz*

*Department of Chemical Engineering, #University of California, Berkeley, and *Chemical Sciences Division, Lawrence Berkeley National Laboratory, Berkeley, California 94720 USA

ABSTRACT The diffusion of hen egg-white lysozyme has been studied by dynamic light scattering in aqueous solutions of ammonium sulfate as a function of protein concentration to 30 g/liter. Experiments were conducted under the following conditions: pH 4–7 and ionic strength 0.05–5.0 M. Diffusivity data for ionic strengths up to 0.5 M were interpreted in the context of a two-body interaction model for monomers. From this analysis, two potential-of-mean-force parameters, the effective monomer charge, and the Hamaker constant were obtained. At higher ionic strength, the data were analyzed using a model that describes the diffusion coefficient of a polydisperse system of interacting protein aggregates in terms of an isodesmic, indefinite aggregation equilibrium constant. Data analysis incorporated multicomponent virial and hydrodynamic effects. The resulting equilibrium constants indicate that lysozyme does not aggregate significantly as ionic strength increases, even at salt concentrations near the point of salting-out precipitation.

NOMENCLATURE

a_1, a_i	monomer, aggregate activity (mol/liter)
A_{ij}	interaction parameter for ij pair (liter/mol)
B_{ij}	osmotic second virial coefficient for ij pair (liter/mol)
c_p	protein concentration (mol/liter)
$\bar{D}$	z-average apparent diffusion coefficient (cm^2/s)
D_0	zero-angle infinite-dilution diffusion coefficient (cm^2/s)
D_i	diffusion coefficient of an i-mer (cm^2/s)
$D_{i,0}$	infinite-dilution diffusion coefficient of an i-mer (cm^2/s)
$(dn/dc)_{T,p}$	refractive-index increment (ml/g)
e	electron charge ($= 1.602 \times 10^{-19}$ C)
f_0	infinite dilution hydrodynamic friction factor
f_i	ellipsoidal-aggregate hydrodynamic friction factor
$F(r,\sigma_i')$	hydrodynamic interaction function for a solution of monodisperse spheres
$g^E(\tau)$	electric field autocorrelation function
H	Hamaker constant (J)
I	ionic strength of added salt (mol/liter)
k_B	Boltzmann's constant ($= 1.38 \times 10^{-23}$ J/K)
K	nonideal indefinite isodesmic association equilibrium constant (liter/mol)
M, M_i	monomer, aggregate molecular weights (g/mol)
n	refractive index
N_A	Avogadro's number ($= 6.02 \times 10^{23}$ mol^{-1})
q	scattering-vector magnitude ($= 4\pi n/\lambda_{laser} \cdot \sin(\theta/2)$) ($cm^{-1}$)
Q	second central moment of diffusion coefficient distribution
r_0	infinite-dilution hydrodynamic radius (Å)
r_x	crystallographic monomer unhydrated radius (Å)
Δr	effective-sphere hydration/Stern layer thickness (Å)
S_{ij}	multicomponent diffusion hydrodynamic interaction parameter for ij pair
T	absolute temperature (K)
W	potential of mean force (J)
z_1, z_i	monomer, aggregate valence

Greek symbols

α_x, β_x	crystallographic monomer ellipsoidal major, minor semiaxis (Å)
α_i, β_i	effective ellipsoidal aggregate major, minor semiaxis (Å)
γ_i	activity coefficient of i-mer
ϵ	effective-ellipsoid hydration/Stern layer thickness (Å)
ϵ_0	dielectric permittivity of vacuum ($= 8.854 \times 10^{-22}$) (C^2/N Å^2)
ϵ_r	dielectric constant of water ($= 78.54$ at 298 K)
ξ_i	ion-aggregate average radius (Å)
η_0	salt solution viscosity (cp)

Received for publication 13 March 1997 and in final form 11 September 1997.

Address reprint requests to Dr. Harvey W. Blanch or Dr. John M. Prausnitz, Department of Chemical Engineering, 201 Gilman Hall, University of California–Berkeley, Berkeley, CA 94720. Tel.: 510-642-1387; Fax: 510-642-4778; E-mail: blanch@cchem.berkeley.edu.

Ms. Heyer's present address is Institut für Verfahrenstechnik, Technical University, Munich, Germany.

Mr. Rämsch's present address is Institut für Enzymtechnologie, University of Düsseldorf, KFA-Jülich, Düsseldorf, Germany.

Ms. Fornefeld's present address is Institut für Thermo und Fluiddynamik, University of Bochum, Bochum, Germany.

0006-3495/97/12/3211/14 $2.00

θ	scattering angle
κ	inverse Debye length ($Å^{-1}$)
λ	slope of the normalized concentration-dependent diffusion coefficient
λ_{laser}	laser wavelength (= 488×10^{-7} cm)
Λ_{ii}	multicomponent diffusion hydrodynamic interaction parameter for *ii* pair
$\bar{v}$	partial specific volume of lysozyme (= 0.703 ml/g)
Π	osmotic pressure ($J \cdot Å^{-3}$)
Π_{id}	ideal osmotic pressure (= $\rho_s k_B T$) ($J \cdot Å^{-3}$)
ρ_s	total ion number density ($Å^{-3}$)
σ_1, σ_i	monomer, aggregate unhydrated diameter (Å)
σ_1', σ_i'	monomer, aggregate hydrated diameter (Å)
$\overline{\sigma_{ion}}$	average ion diameter (Å)
ϕ	protein volume fraction
Φ_{osm}	osmotic coefficient (= Π/Π_{id}).

INTRODUCTION

Protein precipitation and crystallization are key steps in the recovery and characterization of virtually all proteins. In industry, salt-induced protein precipitation is frequently used as a first-pass purification step (Scopes, 1994; Rothstein, 1994), and in research, large, high-quality crystals are required for structure determination and studies of structure-function relationships. For these applications, predictive models based on fundamental protein properties would be of considerable benefit. Because precipitation and crystallization are both aggregation processes driven by intermolecular interactions, it is crucial to understand how equilibrium interactions depend on experimental variables (e.g., protein concentration and purity, salt identity, ionic strength, pH, and temperature). Recent work in this area has focused on correlating precipitation and crystallization data with molecular quantities such as the potential of mean force between protein monomers (Tavares and Sandler, 1997; Rosenbaum et al., 1996; Chiew et al., 1995; Mahadevan and Hall, 1992; Vlachy et al., 1993) and the osmotic second virial coefficient (George and Wilson, 1994). In this paper we report the results of light-scattering measurements of the diffusion coefficient and the extent of aggregation in solutions of a common protein, hen egg-white lysozyme, with the salt concentration varying between dilute and near-salting-out conditions.

Hen egg-white lysozyme is a robust, compact globular protein that is soluble over a broad range of conditions. It is available at high purity and has been studied extensively, making it suitable for the investigation of protein-solution behavior. Previous equilibrium-sedimentation experiments have shown that at low concentrations, hen egg-white lysozyme undergoes a reversible pH-dependent aggregation in solutions of low ionic strength (Sophianopoulos and Van Holde, 1961). At pH below 4.5, lysozyme is monomeric, whereas at higher pH, increasing aggregation is observed. This aggregation follows from an attractive interaction between Glu^{35} in the active site (Glu^{35} has an unusually high pK_a, ~6.3) and Trp^{62}, with equilibrium aggregates growing in a "head-to-tail," chainlike structure (Norton and Allerhand, 1977; Banerjee et al., 1975; Sophianopoulos, 1969; Blake et al., 1967; Rupley et al., 1967). Other equilibrium studies of lysozyme aggregation at higher (but undersaturated) concentrations have been interpreted using either monomer-dimer equilibria or models including higher aggregates (Deonier and Williams, 1970; Adams and Filmer, 1966; Bruzzesi et al., 1965). Wills et al. (1980) performed ultracentrifugation experiments with lysozyme at concentrations to 60 mg/ml at pH 8.0; they analyzed their data in the context of an indefinite isodesmic association, concluding that aggregates up to decamers contributed significantly.

Many experimental investigations of lysozyme aggregation have been reported in the protein-crystallization literature in the last decade, for both supersaturated and undersaturated solutions in typical crystallizing solvents (e.g., 2–4% sodium chloride by weight, acetate-buffered at pH 4.2–4.6). It remains an open question whether lysozyme forms large aggregates when undersaturated or when in the prenucleation phase of crystallization. Recent data that support aggregation are from small-angle neutron scattering (SANS) experiments (Niimura et al., 1995; Boué et al., 1993) and dialysis kinetics (Wang et al., 1996; Wilson et al., 1993, 1996). In contrast, some dynamic light-scattering (DLS) studies have concluded that scattering data that may suggest, at first examination, the formation of aggregates, are more accurately explained in terms of interparticle interactions (Muschol and Rosenberger, 1996; Eberstein et al., 1994). DLS is a powerful tool for investigating intermolecular interactions and the aggregation of proteins over a broad range of solution conditions (Shen et al., 1995; Thibault et al., 1992; Skouri et al., 1991, 1992; Murphy et al., 1991; Mikol et al., 1990).

We report here the results of DLS measurements at 25°C for hen egg-white lysozyme at concentrations to 30 g/liter in solutions of the commonly used precipitating salt ammonium sulfate. To examine the regime where aggregation has been reported, pH ranged from 4 to 7. Ionic strength ranged from 0.05 to 5.0 M. Solutions of high ionic strength were studied to obtain insight into interactions between proteins at solution conditions near precipitation. DLS data at low ionic strength were interpreted in the context of a model that relates the measured diffusion coefficients to a two-body potential of mean force between protein monomers (Phillies, 1995). From this analysis, two molecular interaction parameters, the protein effective charge and Hamaker constant, were obtained for the monomer. At higher ionic strength, the model was generalized to account for aggregation by introducing an indefinite isodesmic association reaction, with a corresponding multicomponent diffusion model for polydisperse systems of interacting particles (Batchelor, 1983). From this model, effective equilibrium aggregation constants were found to be zero at ionic strengths up to 5.0 M, indicating that lysozyme does not aggregate significantly, even when the salt concentration approaches protein precipitation conditions (Coen et al., 1995).

MATERIALS AND METHODS

Lysozyme purification

Two grades of hen egg-white lysozyme were obtained from Sigma (St. Louis, MO) and stored dessicated at −5°C. The first (L-2879, lot 15H7090, CAS [52219-07-5]) was lysozyme chloride (crystallized three times, neither dialyzed nor lyophilized), containing ~90% protein by weight, with the remainder as sodium acetate and sodium chloride. The enzymatic activity of this grade was 65,000 units/mg. The second grade (L-6876, lots 111H7010 and 53H7145, CAS [12650-88-3]) contained lysozyme (crystallized three times, dialyzed, and lyophilized, ~95% protein by weight, with the remainder sodium acetate and sodium chloride, and specific activity of 50,000 units/mg). For the experiments with ionic strength to 1.0 M, lysozyme L-2879 was purified by size exclusion chromatography at pH 3 (HCl) in a 5 × 60-cm column packed with Toyopearl HW50-F (Supelco, Bellefonte, PA). The central portion of the lysozyme peak was collected, concentrated to 30 mg/ml protein via ultrafiltration, and exhaustively dialyzed against ammonium sulfate solutions of the desired ionic strength. DLS samples with lower protein concentrations were prepared by dilution with an ammonium sulfate solution of the same ionic strength, and pH adjusted with small volumes of conjugate acid or base. All solutions were loaded into DLS sample cells within a few hours of preparation. In the experiments with ionic strength between 3.0 and 5.0 M, lysozyme L-6876 was used as supplied, without further purification.

A.C.S.-grade ammonium sulfate (CAS [7783-20-2]), sulfuric acid (CAS [7664-93-9]), and ammonium hydroxide (CAS [1336-21-6]) were obtained from Fisher Scientific. Distilled, deionized, and 0.2-μm-filtered water was dispensed from a Barnstead NANOpure system.

Dynamic light-scattering measurements

The dynamic light-scattering system consisted of an Innova-90 argon-ion laser (Coherent, Santa Clara, CA) that was vertically polarized, tuned to λ_{laser} = 488 nm, and operating at a output power between 50 and 500 mW; a BI-240SM multiangle goniometer; a BI-EMI-9865 photomultiplier; and a BI-9000 digital autocorrelator (Brookhaven Instruments Corp., Holtsville, NY). The BI-9000 is capable of calculating in real time the electric field autocorrelation function, $g^{E}(\tau)$, that yields z-average diffusion coefficients, $\bar{D}$. Decalin ($C_{10}H_{18}$, Aldrich 29477-2, CAS [91-17-8], refractive index $n \approx 1.47$) was used as an index-matching liquid to reduce flare. The sample temperature was maintained at 25°C (± 0.2°C) with a VWR model 1160 recirculating water bath. Sample cells were precision-ground Pyrex NMR tubes with 12-mm O.D., 0.5-mm wall thickness and n = 1.49 (Wilmad Glass, Buena, NJ), with a volume of 5 ml. After the sample tubes were cleaned, loaded, and sealed in a low-dust environment, the samples were recirculated through an in-line membrane filter cartridge, by using a peristaltic pump, until a dust-free trial autocorrelation function was observed at θ = 30°. Filtration times ranged from 10 to 90 min, and the necessary filter pore size varied: 0.2-μm Millex-GV (Millipore, Bedford, MA), 0.1-μm Millex-VV, or Anotop 0.02-μm (Whatman, Clifton, NJ). UV spectrophotometric assays showed that at the end of each experiment, protein loss due to filtration was less than 5% in all cases. Filtration flows were ~2 ml/min to avoid shear-induced protein denaturation. Subsequent to filtration, the samples were allowed to equilibrate for at least 30 min before data acquisition commenced. At the same time, the index-matching fluid was recirculated through a 47-mm O.D. 0.1-μm pore-size hydrophobic membrane filter (GSEP 047A0; Millipore) until visual inspection indicated dust-free decalin. All components in the decalin-filtration system consisted of solvent-resistant materials: Teflon and Viton tubing, a magnetically coupled gear-pump head with stainless steel and Teflon internals, a stainless steel filter housing, and a quartz index-matching vessel.

In a typical experiment, the scattered-light intensity was measured from 30° to 90° in 10° increments. For each sample, three measurements were made at each angle. Data were collected over a period of 10–30 min, depending on the angle and the protein concentration, with a minimum photon count of 5 × 10^8. Data were rejected if the difference between calculated and measured baselines of the autocorrelation function was greater than 0.02%. The majority of accepted data had baseline agreement of ~0.01%.

To obtain diffusion coefficients from autocorrelation data, the quadratic cumulant expansion analysis was employed (Koppel, 1972). In most cases, the second central moment of the diffusion-coefficient distribution, Q, was small (<0.02), indicating narrow size distributions. For the few cases where Q was greater than 0.02, inversion of the autocorrelation function was performed with Brookhaven Instruments Corporation version of the CONTIN program (Provencher, 1982a,b). BI-CONTIN results routinely indicated narrow unimodal diffusion-coefficient distributions centered near the value of $\bar{D}$ given by the quadratic cumulant result. Salt-scattering effects were eliminated by discarding the first few autocorrelator channels when distribution analyses were performed. The data were time-independent over the course of a run, typically ~5 h. Frequent checks were made by repeating the measurements at θ = 30° after completing measurements at θ = 90°; no significant differences were observed, indicating that the samples were in a stationary state over the time scale of these experiments. Protein concentrations were sufficiently low that multiple scattering effects were not considered.

At the conclusion of each DLS experiment, protein concentrations were determined by measuring absorbance at 280 nm and 25°C with a Beckman DU-6 spectrophotometer. The extinction coefficient used for lysozyme was 2.635 liters/(g-cm) (Sophianopoulos and Van Holde, 1964). The refractive index of each sample was measured with a Zeiss refractometer using white light. Refractive indices increased linearly with lysozyme concentration; the observed refractive index increment, $(dn/dc)_{T,p}$, was 0.18 ml/g, a typical value for most proteins.

RESULTS

Light-scattering experiments were conducted over the pH range of 4–7, with ammonium sulfate ionic strength between 0.05 and 5.0 M and lysozyme concentration between 5 and 30 mg/ml. At each pH and ionic strength, three protein concentrations were examined over the angular range of 30°–90°. Fig. 1 shows a typical dynamic Zimm plot (Stepanek, 1993) where, for a given pH and ionic strength,

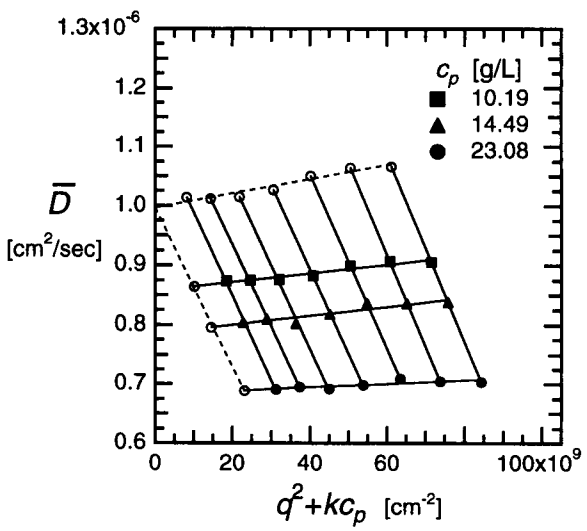

FIGURE 1 Dynamic Zimm plot for hen egg-white lysozyme in ammonium sulfate: I = 4.0 M, pH 6.1. Filled symbols represent DLS data; open symbols are extrapolations to zero angle or zero concentration. D_0 is given by the intersection of the (*dotted*) least-squares lines through the extrapolated values. Plotting constant k = 10^9.

the average apparent diffusion coefficient $\bar{D}$ (in cm^2/s), obtained from DLS autocorrelation data, is plotted for each protein concentration as a function of the parameter $q^2 + kc_p$, which depends both on the scattering angle [$q \approx \sin(\theta/2)$] and on the total molar concentration of protein, c_p. The extrapolated value of $\bar{D}$ is the infinite-dilution zero-angle self-diffusion coefficient, D_0, corresponding to the diffusion of an isolated monomer. Diffusion coefficient data are compiled in Table 1. In Fig. 1, as in all experiments, the measured values of $\bar{D}$ show little dependence on the magnitude of the scattering vector, q, suggesting that samples in these experiments contained narrow unimodal distributions of small oligomers.

Infinite-dilution diffusivities

Fig. 2 shows infinite-dilution hydrodynamic radii, r_0 (in Å), obtained from dynamic Zimm plots via the Stokes-Einstein equation for infinitely-dilute monodisperse spheres:

$$D_0 = \frac{k_B T}{f_0} = \frac{k_B T}{6\pi\eta_0 r_0} \cdot 10^{17} \quad (1)$$

TABLE 1 Diffusion coefficients, $\bar{D}$, of lysozyme in ammonium sulfate solutions, obtained from Zimm plots measured by dynamic light scattering at 25°C

I (M)	pH	ϕ (· 10^3)	$\bar{D}$ (· 10^6) (cm^2/s)	I (M)	pH	ϕ (· 10^3)	$\bar{D}$ (· 10^6) (cm^2/s)	I (M)	pH	ϕ (· 10^3)	$\bar{D}$ (· 10^6) (cm^2/s)
0.05	4.25	0	1.298		0.30	0	1.305	3.0	4.15	0	1.114
		6.2	1.322			5.6	1.211			6.8	0.995
		12.3	1.345			12.2	1.123			13.1	0.885
		17.4	1.365			18.9	1.001			19.6	0.770
	4.9	0	1.277	0.4	4.15	0	1.294		4.9	0	1.099
		6.2	1.279			6.3	1.230			6.6	0.986
		12.9	1.283			13.4	1.167			13.1	0.874
		18.0	1.285			20.4	1.092			19.3	0.765
	6	0	1.370	0.50	4.02	0	1.332		6.9	0	1.056
		5.6	1.334			6.5	1.247			6.9	0.954
		11.4	1.300			13.3	1.152			13.8	0.853
		17.3	1.259			20.7	1.059			22.1	0.730
	6.86	0	1.267		5.22	0	1.378	4.0	4.15	0	1.053
		6.0	1.229			6.6	1.282			7.2	0.860
		12.0	1.171			14.5	1.141			9.4	0.799
		21.8	1.113			19.5	1.090			9.7	0.792
0.15	4.09	0	1.348		6.00	0	1.336		4.95	0	1.020
		5.8	1.305			7.2	1.250			6.7	0.880
		12.0	1.259			15.5	1.111			9.8	0.818
		18.5	1.210			24.4	1.020			16.4	0.682
	5.13	0	1.380		6.9	0	1.337		6.1	0	0.998
		5.8	1.305			6.1	1.230			7.2	0.861
		11.7	1.220			12.9	1.086			10.2	0.803
		18.1	1.142			19.7	0.976			16.2	0.687
	6	0	1.354	0.75	4.05	0	1.290		6.9	0	0.980
		5.5	1.279			7.4	1.198			6.8	0.853
		11.7	1.184			15.8	1.092			13.4	0.729
		18.3	1.097			24.2	0.990			19.1	0.624
	6.9	0	1.350	1.0	3.97	0	1.340	5.0	6.9	0	0.911
		4.9	1.289			6.7	1.252			6.0	0.724
		11.2	1.164			13.2	1.153			7.9	0.664
		17.5	1.102			20.4	1.063			8.3	0.650
0.30	4.15	0	1.306		5.03	0	1.355				
		5.9	1.250			6.5	1.262				
		12.0	1.176			13.5	1.159				
		19.5	1.111			19.7	1.070				
	5.03	0	1.342		6.15	0	1.361				
		6.2	1.265			7.1	1.250				
		13.5	1.169			14.7	1.129				
		16.8	1.132			21.8	1.020				
	5.97	0	1.309		6.89	0	1.276				
		6.2	1.236			6.1	1.204				
		13.4	1.132			13.2	1.085				
		20.5	1.058			20.9	1.008				

All $\bar{D}$ values reflect extrapolation to zero scattering angle, and $\bar{D}$ values at zero volume fraction are infinite-dilution extrapolations, D_0. Here, I = ionic strength.

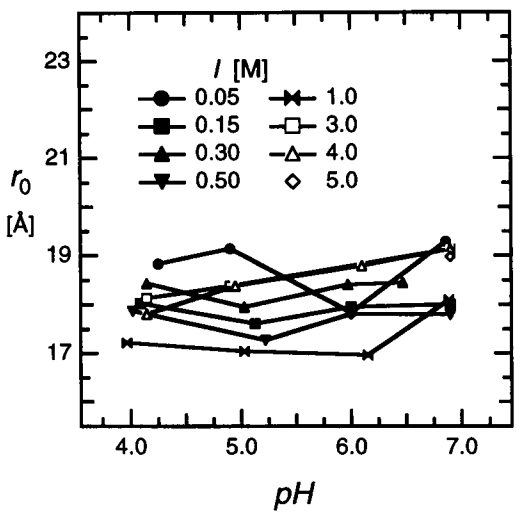

FIGURE 2 Infinite-dilution hydrodynamic radii of lysozyme obtained from Stokes-Einstein relation. The average r_0 at pH 4 is 18 Å (± 0.5 Å).

where f_0 is the hydrodynamic friction factor, k_B is Boltzmann's constant, T is absolute temperature, and η_0 is the viscosity of the solvent (in centipoise). Values for η_0 as a function of ammonium sulfate ionic strength at 20°C were taken from the literature (Weast, 1981) and corrected for temperature.

At pH 4, the average value for r_0 is 18 Å (± 0.5 Å), in good agreement with DLS measurements reported previously for lysozyme at low pH in various salt solutions by Nicoli and Benedek (1976), who calculated from DLS measurements a hydrodynamic radius of 18.5 Å over a pH range of 1.2–2.3 in solutions of 0.2 M potassium chloride, where lysozyme is entirely monomeric. Mikol and co-workers (1990) determined the hydrodynamic radius of lysozyme to be 19.1 Å in solutions of ammonium sulfate at ionic strengths between 6 and 9 M, buffered to pH 4.6 with 40 mM sodium acetate. Eberstein et al. (1994) reported a radius of 20.9 Å in solutions of 0.1 M sodium acetate buffered to pH 4.2, with additional sodium chloride concentrations up to 1.4 M. Muschol and Rosenberger (1995) found a radius of 19 Å for lysozyme in solutions of sodium chloride and acetate at pH 4.7, with total salt concentrations to 0.5 M. Skouri and co-workers (1992) reported r_0 = 22 Å in solutions of sodium chloride, buffered to pH 4.6 with 40 mM sodium acetate, over the temperature range 13°–22°C. The differences in the above-mentioned literature values for the hydrodynamic radius may reflect differences in experimental technique and the use of different salts and ionic strengths in each of those studies. Protein concentration effects may also be reflected in those data because the radii reported were not all obtained from infinite-dilution diffusivities. Furthermore, other protein impurities may have been present in the lysozyme used in those experiments.

Lysozyme hydrodynamic radii obtained from DLS are slightly larger than the equivalent spherical radius, r_x, of the unhydrated lysozyme monomer, as determined by x-ray crystallography at pH near 4. The crystal structure of hen egg-white lysozyme (Brookhaven protein database structure 2LYZ) shows that the unhydrated monomer is a prolate ellipsoid of revolution with major semiaxis α_x = 22.5 Å and symmetrical minor semiaxes β_x = 15 Å, corresponding to r_x = 17.2 Å. Surrounding the lysozyme molecule are bound water molecules that diffuse with the protein; these bound water molecules are therefore reflected in the diffusivities measured by DLS. Close to the surface of the protein are salt ions that may either bind tightly, because of specific salt-protein interactions (within the Stern layer), or associate more loosely within the Gouy-Chapman layer. These ions also affect the measured diffusivities. Although the extrapolation of the dynamic Zimm plot yields D_0 values that reflect the absence of protein-protein interactions, specific salt-protein (ion-binding) and water-protein (hydration) effects remain. In general, for a given protein, these interactions depend strongly on the identity and ionic strength of the salt and, to a lesser degree, on pH (Arakawa and Timasheff, 1982; Melander and Horvath, 1977). The difference between the measured infinite dilution hydrodynamic radius and the crystal structure effective radius is defined here as $r_0 - r_x = \Delta r$; it is assumed to account for hydration and ions bound in the Stern layer and is further assumed to be constant over the ranges of ionic strength and pH investigated. For the data shown in Fig. 2, the average value of Δr over all solution conditions is ~0.8 Å. The values of r_0 show no clear dependence on ionic strength, indicating qualitatively that salt-protein interactions do not change significantly within the range of salt concentrations investigated. Similarly, no effect of pH on the infinite-dilution data was observed, confirming that the extrapolated values are truly free of protein-protein interaction effects.

Concentration-dependent diffusivities

Fig. 3 illustrates the dependence of the normalized average apparent diffusion coefficient, $\bar{D}/D_0$, on protein concentration and pH for several values of ionic strength and pH. Here, $\bar{D}$ at each protein concentration is the zero-angle extrapolated value. Protein concentration is expressed as volume fraction, given by $\phi = c_p M\bar{v}/1000$, where the molecular weight of lysozyme M = 14,600 g/mol, and the partial specific volume $\bar{v}$ = 0.703 ml/g (Sophianopoulos et al., 1962). In all experiments reported here, a linear relationship is observed between $\bar{D}/D_0$ and ϕ, with a slope that varies with solution pH and ionic strength. The slope, λ, contains information about interactions between proteins; for monodisperse (i.e., nonaggregating) systems, formal relationships between λ and the potential of mean force (PMF) are available (Phillies et al., 1995; Batchelor, 1983; Felderhof, 1978). For repulsive interactions, λ is positive, whereas for strong attractive interactions, λ is negative.

As shown in Fig. 3 *a*, λ decreases with increasing ionic strength at pH 4, first making a transition from positive to negative between 0.05 M and 0.15 M, then plateauing at 0.5

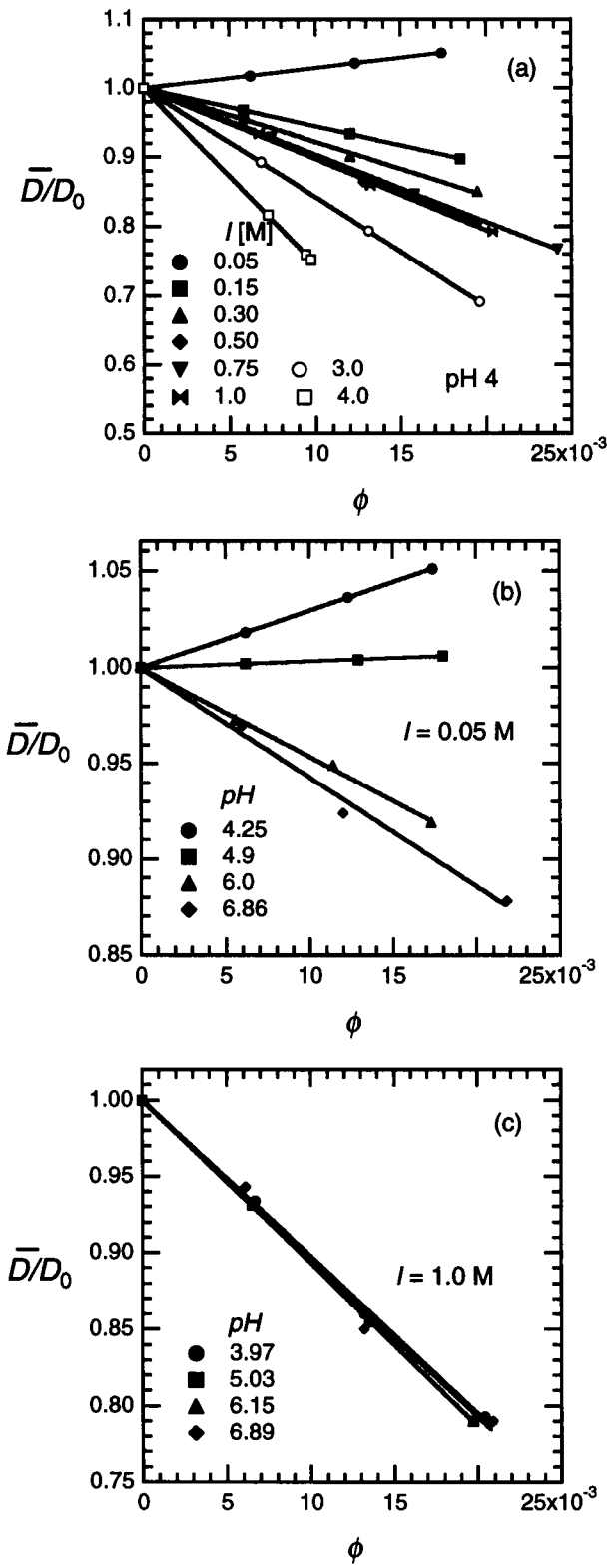

FIGURE 3 Normalized diffusion coefficients of lysozyme in ammonium sulfate solutions as a function of ϕ, the protein volume fraction. (*a*) Ionic strength dependence at pH 4. (*b*) pH dependence at I = 0.05 M. (*c*) pH dependence at I = 1.0 M.

M, then exhibiting a further decrease for ionic strength greater than 1.0 M. A similar dependence of λ on ionic strength was observed for pH 5–7. Fig. 3 *b* shows that λ also depends strongly on pH at low ionic strength. However, as ionic strength increases, the pH dependence is gradually lost (see Fig. 3 *c*). The data in Fig. 3 indicate that a shift occurs in the balance of interactions between lysozyme monomers, from net repulsion at low pH and low ionic strength, toward greater attraction as either pH or ionic strength (or both) increases.

The plateau in λ with increasing ionic strength shown in Fig. 3 *a* can be readily attributed to screening of electrostatic repulsion between proteins, as described in detail in the following section. However, the further decrease in λ as ionic strength exceeds 1.0 M suggests the presence of other ionic-strength-dependent interaction(s) that contribute significantly at higher salt concentrations. The decrease in λ could also indicate aggregation of lysozyme; for solutions of such high ionic strength, approaching the salt concentration where protein precipitation is induced, one might expect to observe large equilibrium clusters of protein molecules. However, for solutions in which concentration-dependent aggregation were to occur, the dependence of $\bar{D}/D_0$ on protein concentration would not be linear, because of the presence of particles of different sizes. Therefore, the linear nature of the data for ionic strength greater than 1.0 M suggests that significant aggregation does not occur in these solutions.

DISCUSSION

The potential of mean force

Protein interactions can be described quantitatively by a two-body potential of mean force; three-body and higher interactions become important at protein concentrations higher than those reported here. Selection of the proper form of the potential of mean force requires knowledge of the dominant physical interactions between proteins in equilibrium solutions. In low-ionic-strength solutions, proteins interact primarily through a balance of electrostatic repulsion and attractive dispersion forces that can be described, for example, by the Derjaguin–Verwey–Landau–Overbeek (DLVO) theory (Verwey and Overbeek, 1948). However, in high-ionic-strength solutions, where salt-induced protein precipitation occurs, macromolecular coulombic interactions are essentially screened and the overall interaction is attractive. Furthermore, because the salt concentration is so high, ion-excluded-volume effects become significant. The following multicomponent potential-of-mean-force model accounts for all of these phenomena in aggregating lysozyme solutions. A one-component potential of mean force has been used previously to describe osmotic pressure data (Vlachy et al., 1993) and precipitation phase equilibrium results (Tavares and Sandler, 1997); a similar form is applied here to obtain from DLS data two potential parameters specific for lysozyme. The multicomponent form is used to

estimate aggregate-size distributions from the high-ionic-strength data, as described below.

For simplicity in PMF modeling, lysozyme monomers and oligomers are considered effective spheres. The centrosymmetric potential of mean force between an i-mer and a j-mer, $W_{ij}(r)$, is considered here to be the sum of four contributions:

$$W_{ij}(r) = W_{ij}^{HS}(r) + W_{ij}^{elec}(r) + W_{ij}^{disp}(r) + W_{ij}^{osm}(r) \quad (2)$$

The hard-sphere potential, $W_{ij}^{HS}(r)$, is

$$W_{ij}^{HS}(r) = \begin{cases} \infty & r \le \sigma'_{ij} \\ 0 & r > \sigma'_{ij} \end{cases} \quad (3)$$

where $\sigma'_{ij} = (\sigma'_i + \sigma'_j)/2$; σ'_i and σ'_j are the hydrated effective hard-sphere diameters of oligomers i and j, i.e., $\sigma_i + 2\Delta r$ and $\sigma_j + 2\Delta r$. The effective hard-sphere diameters for protein aggregates are estimated by considering the "head-to-tail" nature of the lysozyme aggregation, described earlier, and the crystal structure of lysozyme. Aggregates were considered to have a simplified effective ellipsoidal geometry, shown in Fig. 4 for a dimer, with hydrated major and minor semiaxes α'_i and β', respectively. For an aggregate thus described as a rigid prolate ellipsoid of revolution, the hydrodynamic friction factor, f_i, is given by (Zero and Pecora, 1985)

$$f_i = 6\pi\eta_0\alpha_i \frac{(1-\rho_i^2)^{0.5}}{\ln\{[1+(1-\rho_i^2)^{0.5}]/\rho_i\}} \quad (4)$$

where $\rho_i = \beta'/\alpha'_i$. Equating this friction factor with that of the equivalent hydrated effective sphere, $3\pi\eta_0\sigma'_i$, with the assumption of noninterpenetrating hydration/Stern layers of thickness Δr, yields the unhydrated aggregate effective hard-sphere diameter, σ_i. The ellipsoidal aggregate hydrated semiaxes are defined as $\alpha'_i = i \cdot \alpha_x + \epsilon$ and $\beta' = \beta_x + \epsilon$, where ϵ is the thickness of the hydration/Stern layer around the aggregate; ϵ is estimated from infinite-dilution data by equating the ellipsoidal friction factor for a hydrated monomer, i.e., f_1, with that of the corresponding effective spherical monomer, $6\pi\eta_0(r_x + \Delta r)$. For $\Delta r = 0.8$ Å, $\epsilon = 0.6$ Å and is assumed to be constant over the ranges of ionic strength and pH investigated. This method is reasonable for small rigid linear aggregates; for large aggregates, a worm-like chain or rod model for the friction factor would be more appropriate.

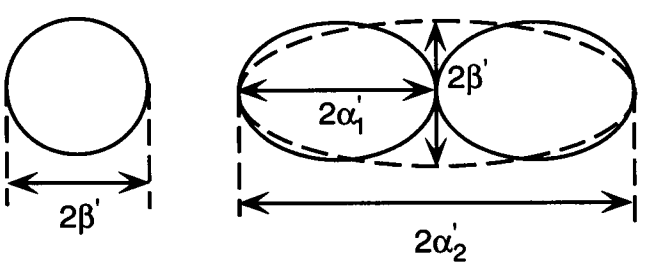

FIGURE 4 Effective ellipsoidal aggregate structure for a hydrated lysozyme dimer.

The repulsive electrostatic interaction, $W_{ij}^{elec}(r)$, is given by

$$W_{ij}^{elec}(r) = \frac{z_i z_j e^2 \exp[-\kappa(r-\sigma_{ij})]}{4\pi\epsilon_0\epsilon_r \cdot r \cdot (1+\kappa\sigma_i/2)(1+\kappa\sigma_j/2)} + \left(\frac{P_i z_i^2}{2} + \frac{P_j z_j^2}{2}\right) \cdot \frac{e^2}{4\pi\epsilon_0\epsilon_r} \quad (5)$$

for $r \ge \sigma'_{ij}$, where z_i is the pH-dependent valence of the i-mer; e is the unit charge; κ is the Debye screening parameter, given by $\kappa^2 = (2e^2N_AI)/(k_BT\epsilon_0\epsilon_r)$; ϵ_0 is the dielectric permittivity of the vacuum; ϵ_r is the dielectric constant; and N_A is Avogadro's number. The P terms, recently introduced by Sushkin and Phillies (1995), incorporate into $W_{ij}^{elec}(r)$ the effects of charge-induced dipole forces and of double-layer distortion around each protein molecule caused by the presence of the other protein. These effects both contribute additional repulsion between proteins. For proteins in aqueous salt solutions, Sushkin and Phillies have shown that, at very small particle separations ($r \le 1.2\sigma_{ij}$), the P terms of $W_{ij}^{elec}(r)$ are larger in magnitude than the Debye-Hückel charge-charge contribution (the first term in Eq. 5), even for solutions of high ionic strength. The ionic strength due to added electrolyte is given by $I = 0.5 \cdot \Sigma c_m z_m^2$, where c_m and z_m are the molar concentration and valence of ion m, respectively. The protein and its counterions are neglected in calculating the ionic strength. The protein monomer valence, z_1, is a parameter of the model regressed from the low-ionic-strength data, as described later. Because the isoelectric point of lysozyme is 11.1, the protein has a positive charge at all conditions studied here.

The unretarded attractive dispersion potential, $W_{ij}^{disp}(r)$, for spherical particles (Hamaker, 1937), for $r \le \sigma'_{ij}$, is

$$W_{ij}^{disp}(r) = -\frac{H}{12}\left\{\frac{\sigma_i\sigma_j}{r^2-\sigma_{ij}^2} + \frac{\sigma_i\sigma_j}{r^2-(\sigma_i-\sigma_j)^2/4} + 2\cdot\ln\left[\frac{r^2-\sigma_{ij}^2}{r^2-(\sigma_i-\sigma_j)^2/4}\right]\right\} \quad (6)$$

where H is the Hamaker constant for the interaction between the i-j pair. Because H is primarily a function of the chemical composition of the protein molecules, it is assumed to be the same for all protein aggregates in solution. Furthermore, H is expected to decrease only slightly, because of dielectric screening as the ionic strength increases to 5.0 M (Israelachvili, 1992). Equation 6 diverges in the limit of particle contact, i.e., $r = \sigma_{ij}$. Hence the assumption of a noninterpenetrating hydration/Stern layer of thickness Δr (obtained from infinite-dilution data) preserves the applicability of Eq. 6. The effective Hamaker constant is a model parameter and is determined here from low-ionic-strength DLS data.

In concentrated electrolyte solutions, ions occupy a significant fraction of the total solution volume. When two

protein molecules or aggregates approach contact, ions are excluded from a region between the protein particles. This causes an imbalance in the local osmotic pressure exerted by the ions on the proteins, approximated by the osmotic pressure of the corresponding protein-free salt solution, $\Pi = \Phi_{osm}\Pi_{id} = \Phi_{osm} \cdot (\rho_s k_B T)$, where ρ_s is the total ion number density and Φ_{osm} is the osmotic coefficient of the ammonium-sulfate solution (Clegg et al., 1996). The result is a strong short-range attractive potential between the proteins, expressed by (Mahadevan and Hall, 1992)

$$W_{ij}^{osm}(r) = \begin{cases} \dfrac{-2\pi}{3} \cdot \Pi \cdot (\xi_i^3 + \xi_j^3) \cdot \\ \cdot \left[1 + \dfrac{r^3}{8(\xi_i^3 + \xi_j^3)} - \dfrac{3r}{4}\dfrac{(\xi_i^2 + \xi_j^2)}{(\xi_i^3 + \xi_j^3)} - \dfrac{3}{8r}\dfrac{(\xi_i^2 - \xi_j^2)^2}{(\xi_i^3 + \xi_j^3)}\right] & \sigma_{ij}' \le r \le \sigma_{ij}' + \overline{\sigma_{ion}} \\ 0 & r > \sigma_{ij}' + \overline{\sigma_{ion}} \end{cases} \quad (7)$$

The ion-oligomer radius $\xi_i = (\sigma_i' + \overline{\sigma_{ion}})/4$, where $\overline{\sigma_{ion}}$ is the average hydrated ion diameter (Horvath, 1985). In this contribution to the overall potential of mean force, the ions are hard spheres; electrostatic effects are assumed to be taken into account in $W_{ij}^{elec}(r)$.

Fig. 5 *a* illustrates the magnitude of the contributions to the potential of mean force for protein monomers, as a function of particle separation r. At 0.05 M ionic strength, electrostatic repulsion is strong, and there is a significant barrier to aggregation. However, because of the strength of the attractive dispersion interaction at small separations, the overall potential becomes slightly attractive near contact ($r = \sigma_{ij}'$). The salt concentration is sufficiently low that the attractive contribution from ion osmotic effects is negligible; it is not shown. Fig. 5 *b* shows that, as ionic strength increases, the repulsive barrier diminishes because of screening of the repulsive electrostatic contribution and increased osmotic attraction. At the highest ionic strength, 5.0 M, attractive ion osmotic effects contribute significantly when the proteins are near contact. Here, the overall PMF is governed by the dispersion interaction for separations greater than the range of the osmotic attraction contribution. As noted by George and Wilson (1994), in solutions that precipitate (e.g., high salt concentration), the potential of mean force is strongly attractive.

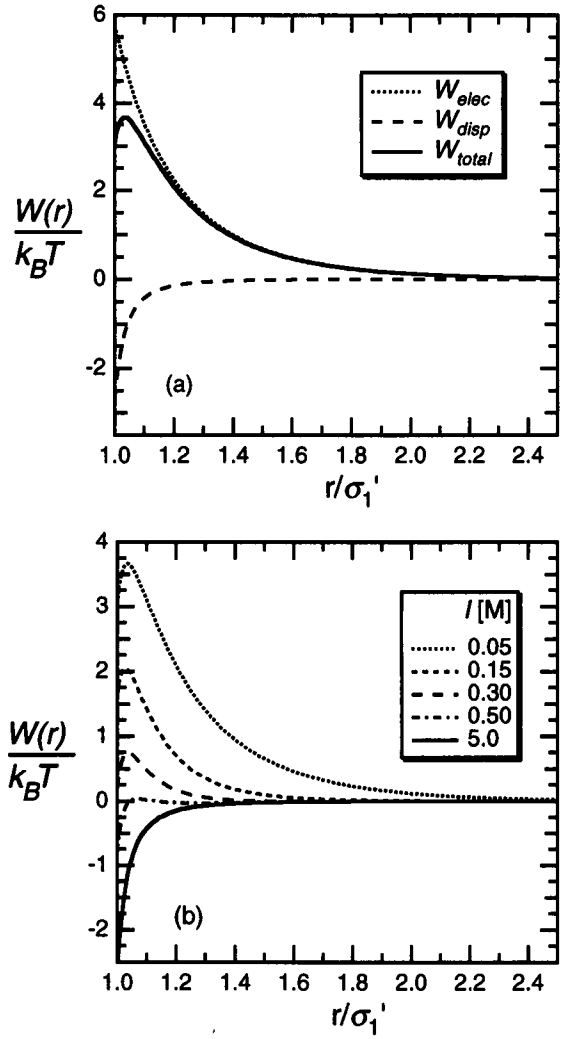

FIGURE 5 (*a*) Contributions to the potential of mean force between two protein monomers ($i = 1$) as a function of reduced distance for $I = 0.05$ M. The solid line represents the total potential of mean force; $W_{ij}^{osm}(r)$ is not shown. (*b*) Dependence of the potential of mean force on ionic strength. Parameters: $z_1 = 10$, $H/k_BT = 5$, $\sigma_1 = 34.4$ Å, $\Delta r = 0.8$ Å, $\overline{\sigma_{ion}} = 6.94$ Å.

Regression of PMF parameters at low pH and ionic strength

All DLS measurements were performed in the long-time, or hydrodynamic, regime, where the time scale of the light-scattering experiment, τ, is much greater than either the intrinsic time scale for Brownian motion or that for direct interparticle interactions (Pusey and Tough, 1985). In this regime, the concentration dependence of the protein diffusion coefficient, λ, may be related quantitatively to the potential of mean force. For systems of monodisperse interacting spheres, λ may be expressed generally as

$$\lambda = \lambda_{HS} + \int_{\sigma_i'}^{\infty} F(r, \sigma_i') \cdot \left[1 - \exp\left(-\frac{W_{ii}(r)}{k_B T}\right)\right] dr \quad (8)$$

where λ_{HS} is a hard-sphere term and $F(r,\sigma_i')$ is a function that takes into account both direct (virial) interparticle forces and hydrodynamic interactions (Russel, et al., 1989). Batchelor (1976), Felderhof (1978), and, most recently, Phillies et al. (1995) provide various forms of $F(r,\sigma_i')$ and values for λ_{HS} (see Table 2), which depend on these authors' different descriptions of hydrodynamic interactions. The result of Phillies is used in this work.

The potential of mean force outlined above contains two adjustable parameters: the Hamaker constant, H, and the

TABLE 2 Hard-sphere contribution to first-order concentration dependence of diffusion coefficient, λ_{HS}, and geometric functions, $F(r, \sigma_i')$, for calculating interparticle interactions in solutions of monodisperse spheres in Brownian motion

Author	λ_{HS}	$F(r, \sigma_i')$
Phillies et al. (1995)	−0.9	$\frac{24r^2}{(\sigma_i')^3} - \frac{12r}{(\sigma_i')^2} + \frac{45\sigma_i'}{8r^2} - \frac{93(\sigma_i')^3}{32r^4} - \frac{225(\sigma_i')^4}{32r^5}$
Felderhof (1978)	1.56	$\frac{24r^2}{(\sigma_i')^3} - \frac{12r}{(\sigma_i')^2} + \frac{15\sigma_i'}{8r^2} - \frac{27(\sigma_i')^3}{64r^4} - \frac{75(\sigma_i')^4}{64r^5}$
Batchelor (1983)	1.45	$\frac{24r^2}{(\sigma_i')^3} - \frac{11.89r}{(\sigma_i')^2} - \frac{0.706}{\sigma_i'} + \frac{1.69}{r}$

protein monomer valence, z_1; both are obtained from the data at pH 4, where the lysozyme is a monomer. For each ionic strength between 0.05 M and 0.5 M, a curve was generated representing the set of $\{H, z_1\}$ points that satisfy the constraint that the experimentally measured λ and the λ calculated from the PMF model are equal. This was achieved by setting H to a constant value and finding the value of z_1 that gave a calculated value of λ (via Eqs. 2–8) equal to the experimentally measured value. These regressions were performed with MathCad Plus 6.0, a symbolic equation-solving software application. Each curve in Fig. 6 was generated stepwise by repeating this procedure over small increments in H. The common intersection of these curves for different ionic strengths occurs at $H/k_BT = 8.9$ and $z_1 = 5.5$. This procedure has been used previously, with various forms of the PMF, to obtain molecular interaction parameters. Corti and Digiorgio (1981) used the DLVO potential of mean force to interpret DLS data in a study of interactions between sodium dodecyl sulfate micelles in solutions of sodium chloride at two ionic strengths. Eberstein et al. (1994) studied diffusion of hen egg-white lysozyme in acetate-buffered (pH 4.2) solutions of sodium chloride at 25°C and pH 4.2 over the ionic strength range of 0.05–1.40 M; they obtained $H/k_BT = 7.6$ and $z_1 = 6.4$. More recently, Muschol and Rosenberger (1995) performed static and dynamic light-scattering measurements on lysozyme in solutions of sodium chloride and sodium acetate at pH 4.7 with a total ionic strength from 0.05 to 0.5 M. Using the same expression for the screened Coulombic repulsion potential as that used by Eberstein et al., they calculated from DLS data the $H/k_BT = 7.2$ and $z_1 = 5.4$.

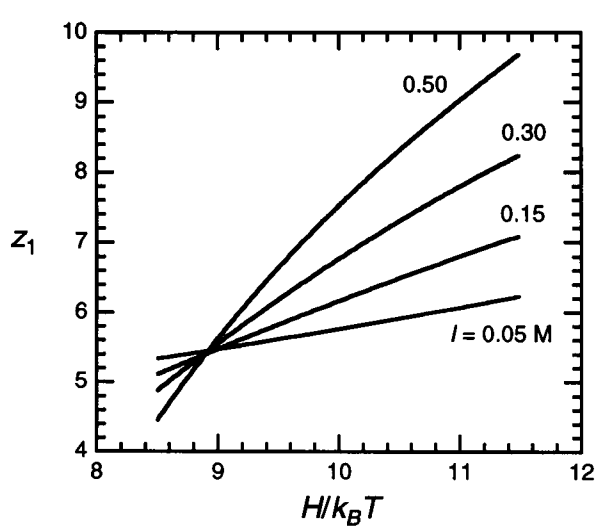

FIGURE 6 Fitting effective monomer charge and Hamaker constant at pH 4 to the experimental data in Fig. 3 *a*. The common intersection of these curves gives the ionic-strength-independent values of H/k_BT and z_1.

The Hamaker constant for the interaction of two colloidal particles depends primarily on their chemical compositions, which determine the magnitude of their overall electronic polarizabilities. It also depends on the dielectric properties of the medium containing the particles. Hence H depends to some extent on the ionic strength of the protein solution. Furthermore, as solution pH changes, the net fixed proton charge of the protein changes; the effect of this change is taken into account by Eq. 5, and the very small effects of pH on H are neglected. We estimate the Hamaker constant for the interaction of two lysozyme monomers, based on Lifshitz theory (Israelachvili, 1992), using average protein dielectric properties, to be $H/k_BT \approx 5$ at low ionic strength, with a decrease of ~5% at 5.0 M ionic strength due to screening of (weak) permanent-dipole effects. This result indicates that assuming the dispersion interaction to be independent of ionic strength is reasonable for calculating H from DLS data. Moreover, this value is in fair agreement with the DLS results presented here and those of other workers cited above. Furthermore, it is consistent with results reported in the literature obtained with other experimental techniques, such as membrane osmometry (Haynes, 1992) and low-angle laser light scattering (Coen et al., 1995; Curtis et al., 1997). Other workers have provided estimates of H by using more complete descriptions of protein shape and composition. For example, Roth and co-workers (Roth et al., 1996) have calculated an effective Hamaker constant for the interaction between bovine serum albumin (BSA) molecules in salt-free water, $H/k_BT = 3.10$.

The regressed value of the lysozyme monomer valence, $z_1 = 5.5$, differs significantly from the titration data reported by Tanford and Wagner (1954), who measured a net proton association of +14 at pH 4 for lysozyme in solutions of potassium chloride at 0.15 M ionic strength. However, Riès-Kautt and Ducruix (1994) have shown that lysozyme binds sulfate anions on the surface. The form of the screened Coulombic repulsion potential used in this work requires the surface charge of lysozyme, which includes both the proton charge and the sum of the charges of the ions in the Stern layer. The loosely bound ions in the diffuse double layer are neglected. Considering the effect of sulfate surface binding, which is assumed to be saturated at 0.05 M

ionic strength, the net charge at pH 4 reported here seems reasonable.

Muschol and Rosenberger (1995) have commented on the sensitivity of this regression method to the value chosen for Δr, which determines the lower limit of the PMF integrations in Eq. 8. The sensitivity arises from the divergent nature of Eq. 6 for the case $\Delta r = 0$, i.e., $r = \sigma_{ij}$. Significantly different results are obtained by allowing Δr to vary slightly, as shown in Fig. 7. For regressing the Hamaker constant and the monomer valence, and performing subsequent calculations of aggregation equilibrium constants at higher pHs, a physical basis for the choice of Δr is required. The value $\Delta r = 0.8$ Å chosen for this work was the average calculated from examining Fig. 2 at pH 4, with the assumption that lysozyme is monomeric at this pH. The average was chosen because no systematic variation in r_0 with ionic strength was observed at pH 4.

To verify this, the regressed values of the Hamaker constant and monomer valence (adjusted for pH using experimental titration data for lysozyme) were used to calculate values of λ for pH 5–7 at ionic strengths between 0.05 and 0.5 M. In all cases the calculated values of λ matched the experimental values within a few percent, indicating that the monomer interaction model describes the data well. This is not necessarily a contradiction of the pH-dependent dimerization equilibrium reported for lysozyme (Sophianopoulos and Van Holde, 1964), because it is generally acknowledged that it is not possible to quantitatively resolve monomers from dimers of such small molecules with DLS. However, if significant aggregation were to occur in these solutions, the monomer model would not describe the normalized diffusion coefficient data of Fig. 3, and aggregates would be detected by DLS.

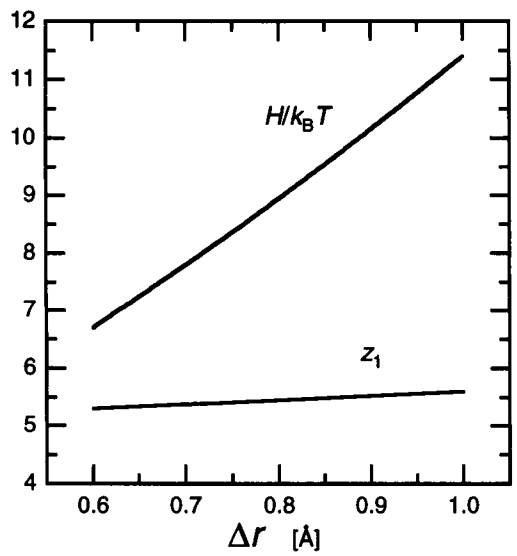

FIGURE 7 Dependence of parameters H/k_BT and z_1 on the value of Δr, the thickness of the hydration/Stern layer, for lysozyme at pH 4. In this work, the value of $\Delta r = 0.8$ Å, giving $H/k_BT = 8.9$ and $z_1 = 5.5$.

A chemical association model for lysozyme aggregation

To quantify aggregation in lysozyme solutions of ionic strength greater than 1.0 M, a nonideal, indefinite, isodesmic association model is applied here. The equilibria are

$$2L_1 \overset{K_2}{\longrightarrow} L_2$$

$$L_2 + L_1 \overset{K_3}{\longrightarrow} L_3 \qquad (9)$$

$$L_3 + L_1 \overset{K_4}{\longrightarrow} L_4, \cdots \text{etc.}$$

Here, L_1 is the lysozyme monomer, L_2 is the dimer, and so on. The equilibrium constant K_i is defined as

$$K_i = \frac{a_i}{a_{i-1}a_1} \qquad (10)$$

where $a_i = \gamma_i c_i$ is the activity of an i-mer. The standard state is an ideal solution of unit concentration; c_i and γ_i are molar concentration and activity coefficient of an i-mer, respectively. For isodesmic association, K_i is assumed to have the same value for all association steps; hence the activity of any i-mer is given in terms of the monomer activity, a_1, and the equilibrium constant, K (in liters/mol), as follows (Wills et al., 1980):

$$a_i = K^{(i-1)}a_1^i \qquad (11)$$

The total molar concentration of protein, c_p, is

$$c_p = \sum_i ic_i = \sum_i iK^{(i-1)}\frac{a_1^i}{\gamma_i} \qquad (12)$$

For dilute and semidilute solutions, the composition-dependent activity coefficient of an i-mer, γ_i, is given by

$$\ln \gamma_i = \sum_j A_{ij}c_j \qquad (13)$$

where the summation is for all solute species, including i. Parameters A_{ij} (in liters/mol) are related to the osmotic second virial coefficients, B_{ij} (also in liters/mol), by

$$A_{ij} = 2B_{ij} - M_j\bar{v}/1000 \qquad (14)$$

where M_j is the molecular weight of a j-mer. The osmotic second virial coefficient for the interaction between an i-mer and a j-mer, B_{ij}, is related to the potential of mean force by

$$B_{ij} = 2\pi N_A \cdot 10^{-27} \cdot \int_0^\infty \left[1 - \exp\left(\frac{-W_{ij}(r)}{k_BT}\right)\right] r^2 dr \qquad (15)$$

where N_A is Avogadro's number and r is in Å.

The equilibrium constant, K, can be calculated from protein-diffusion data obtained by DLS experiments. The experimentally measured quantity is the z-average apparent diffusion coefficient, $\bar{D}$ (Weiner, 1984):

$$\bar{D} = \frac{\sum_i c_i M_i^2 D_i}{\sum_i c_i M_i^2} = \frac{\sum_i M_i^2 K^{(i-1)} a_1^i / \gamma_i D_i}{\sum_i M_i^{2(i-1)} a_1^i / \gamma_i} \quad (16)$$

where D_i is the diffusivity of the i-mer in solution. The diffusion model of Phillies et al. (1995) for interacting spheres has not yet been extended to multicomponent systems. Hence the approximate model of Batchelor is used to describe the diffusion coefficient of each aggregate species in a dilute polydisperse systems of interacting effective spheres (Batchelor, 1983):

$$D_i = D_{i,0}\left[1 + \Lambda_{ii}\phi + \sum_{j \neq i} S_{ij}\phi_j\right] \quad (17)$$

where volume fraction ϕ is given by $c_p\bar{v}/1000$ and the $D_{i,0}$ are the infinite-dilution diffusion coefficients of the i-mers. The $\{\Lambda_{ii}\}$ account for the interactions (virial and hydrodynamic) between aggregates of the same size. The $\{S_{ij}\}$ represent the effects of other aggregate species on the diffusion of an i-mer. These terms also include contributions from both virial and hydrodynamic interactions; they are integral functions of the multicomponent potential of mean force and the aggregate size ratio, σ_j'/σ_i'. The $D_{i,0}$ are approximated by $D_{i,0} = k_B T/f_i$, where the friction factors, f_i, are given by Eq. 4.

The model summarized in Eqs. 9–17 was used to calculate an equilibrium constant, K, from the DLS data for ionic strengths above 1.0 M, using an iterative technique described in the Appendix. In evaluating the multicomponent potential of mean force, the effective Hamaker constant regressed from the low-ionic-strength data was used and was assumed to be identical for all aggregates. The monomer valence at pH 4 was adjusted for pH, using experimental titration data for lysozyme. In all cases, the calculated results indicated no aggregation, confirming the previous hypothesis based on Fig. 3: the diffusion data at all solution conditions reflect only the effects of interparticle interactions between monomers. As noted previously, it is difficult to resolve narrow size distributions of such small particles from DLS data. Hence the general conclusion is that significant aggregation—for example, the formation of preprecipitation aggregates, or "praggs" (Mikol et al., 1990)—does not occur for lysozyme at concentrations to 30 g/liter in ammonium sulfate solutions of ionic strength to 5.0 M.

The absence of preprecipitation aggregates is in accord with the studies of Muschol and Rosenberger (1995), who suggest that many previous scattering studies of lysozyme in crystallization solvents have overestimated protein aggregation by neglecting the effects of attractive intermolecular forces and hydrodynamic interactions (Muschol and Rosenberger, 1996). To illustrate further the importance of accounting for solution nonideality, equilibrium constants were calculated from the DLS data for ionic strengths of 1.0 M and greater, using two additional alternative descriptions of protein particles: 1) effective hard-sphere aggregates with excluded-volume and hydrodynamic interactions, but no attractive potential of mean force, and 2) ideal particles with no hydrodynamic or virial interactions. Fig. 8 shows equilibrium constants calculated from DLS data for these descriptions as a function of ionic strength, for solutions with pH ~7. (Similar results are obtained for pH 4–6.) The values of K calculated from the effective hard-sphere approximation are greater than those resulting from the ideal approximation; when repulsive excluded-volume effects are included, there is a corresponding slight increase in the calculated aggregation equilibrium constant. For both of these approximate descriptions, significant aggregate-size distributions would result from the calculated equilibrium constants, especially at higher ionic strengths, although the diffusion data of Fig. 3 do not reflect aggregate formation. However, when the attractive potential-of-mean-force contributions to the measured diffusion coefficients are included, the resulting calculated equilibrium constants fall to zero, indicating that lysozyme is monomeric, even at ionic strengths up to 5 M. For these calculations, the errors between calculated and measured values of $\bar{D}$ become significant for ionic strengths greater than 3 M, suggesting that the Batchelor model may overestimate the effect of strongly attractive potentials on the hydrodynamic interactions between particles. It remains to be seen whether the hydrodynamic interaction model of Phillies (1995), when generalized to the multicomponent case, will give a more accurate description of the average apparent diffusion coefficient in aggregating systems.

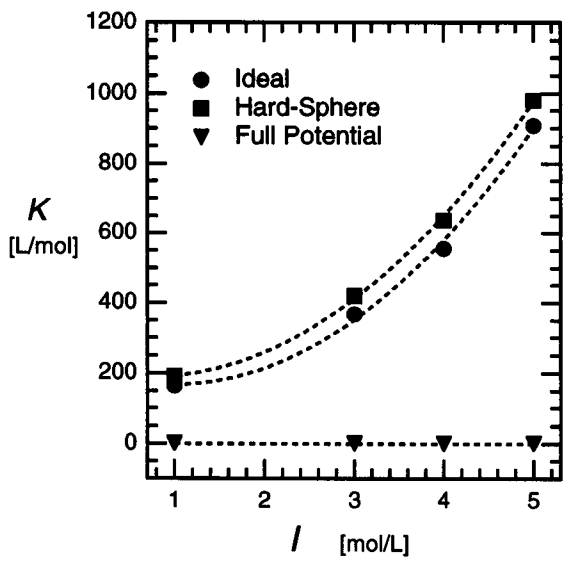

FIGURE 8 Calculated values of the aggregation equilibrium constant, K, as a function of ionic strength at pH 7, for three different descriptions of protein particles: noninteracting ideal particles (*circles*), hard spheres (*squares*), and hard spheres interacting through the potential of mean force $W_{ij}(r)$.

Both the screened electrostatic repulsion and dispersion-attraction potentials rely on a mean-field description of the ions as part of a one-component salt/water pseudosolvent. This approximation is acceptable at very low ionic strengths, but becomes less valid with increasing salt concentration. Applying such an approximate description at ionic strengths greater than 0.1 M is a significant extrapolation. A potential model that accounts explicitly for the size and charge of the salt ions is needed. Accounting for the excluded-volume effects of the ions via the osmotic-attraction potential given in Eq. 7 is only a first approximation. Nevertheless, the multicomponent diffusion-interaction model presented here is likely to be appropriate for the analysis of diffusion data for systems where the solute exhibits an equilibrium aggregate-size distribution wider than that for lysozyme.

CONCLUSION

Dynamic light scattering has been used to study the aggregation of hen egg-white lysozyme in aqueous solutions of ammonium sulfate at 25°C. The concentration dependence of lysozyme apparent diffusion coefficients was interpreted in the context of a two-body potential of mean force that includes repulsive hard-sphere and Coulombic interactions and attractive dispersion and ion osmotic interactions. Analysis of data at low pH for ionic strengths to 0.5 M allowed regression of the effective monomer charge ($z_1 = 5.5$) and the Hamaker constant ($H/k_BT = 8.9$); these were then applied at higher pH and at higher ionic strengths. Calculated equilibrium constants indicate that no aggregation occurred, even at the highest pH and ionic strength. The implication of these results for lysozyme precipitation and crystallization is that lysozyme exhibits a phase transition (which depends on pH, ionic strength, and salt identity) between soluble distributions of small aggregates and large macroscopic clusters, rather than a gradual increase in the aggregation state as ionic strength rises.

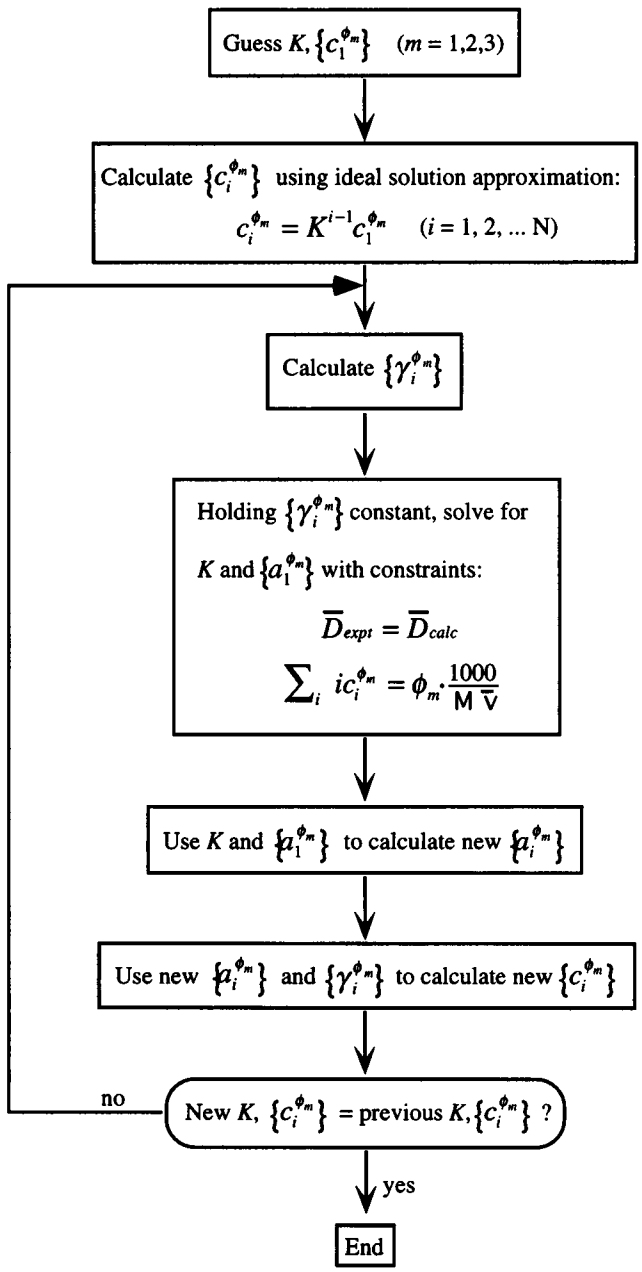

FIGURE 9 Flow diagram for calculating aggregation equilibrium constants from diffusion data.

APPENDIX: CALCULATION SCHEME FOR FITTING AGGREGATION EQUILIBRIUM CONSTANTS

The activity coefficients of the i-mers, $\{\gamma_i\}$, each depend on the concentrations of all aggregates, as described in Eq. 13. As a result of this complex concentration dependence, an iterative method was required to determine K. At each solution condition, K was regressed under the constraint that, for each of the three protein solutions, the difference between the calculated and the experimental values of $\bar{D}$ was minimized, while satisfying the total protein mass balance given in Eq. 12. A flow diagram for this calculation procedure is shown in Fig. 9. In all cases, the mass balances were satisfied exactly, and in most cases the error between the calculated and experimental $\bar{D}$ values was less than 5%.

Calculation of the second virial coefficients, $\{B_{ij}\}$, and the multicomponent hydrodynamic interaction parameters, $\{S_{ij}\}$, required numerical integration to a large upper limit in distance, r, expressed in multiples of σ'_{ij}. In a trial calculation with the longest ranged potential of mean force used in this work (corresponding to pH 4 and $I = 0.05$ M, where screened Coulombic repulsion is the dominant contribution to the overall potential), it was determined that the change in any of these integrated quantities that resulted from changing the upper limit of integration from $r/\sigma'_{ij} = 8$ to $r/\sigma'_{ij} = 9$ was less than 0.01%. Furthermore, the maximum number of possible aggregates considered, N, determined how many virial coefficients needed to be calculated, $N(N + 1)/2$. N is infinite for the indefinite isodesmic aggregation model. For the cases labeled "ideal" and "hard sphere" in Fig. 8, the value of N above which the value of K did not change by more than 0.01% with increasing N was found to be 10. For the case where the attractive potential of mean force was included in the regressions (labeled "full potential" in Fig. 8), the value of N had little effect on the results, because all equilibrium constants were essentially zero; the value used was $N = 4$.

All authors are grateful to Sheldon Oppenheim (University of Iowa) for advice regarding the chromatographic purification of lysozyme.

This work was supported by the National Science Foundation (CTS 95-30793) and by the Director, Office of Energy Research, Office of Basic Energy Sciences, Chemical Sciences Division of the U.S. Department of Energy, under contract DE-AC03-76SF00098. DHK is grateful for support from the National Institutes of Health under a National Institutes of Health National Institute of General Medical Sciences Trainee grant. CH was supported by a scholarship from the Ernst-Solvay Stiftung.

REFERENCES

Adams, E. T., Jr., and D. L. Filmer. 1966. Sedimentation equilibrium in reacting systems. IV. Verification of the theory. *Biochemistry.* 5: 2971–2985.

Arakawa, T., and S. N. Timasheff. 1982. Preferential interactions of proteins with salts in concentrated solutions. *Biochemistry.* 21: 6545–6552.

Banerjee, S. K., A. Pogolotti, and J. A. Rupley. 1975. Self-association of lysozyme. *J. Biol. Chem.* 250:8260–8266.

Batchelor, G. K. 1976. Brownian diffusion of particles with hydrodynamic interaction. *J. Fluid Mech.* 74:1–29.

Batchelor, G. K. 1983. Diffusion in a dilute polydisperse system of interacting spheres. *J. Fluid Mech.* 131:155–175.

Blake, C. C. F., L. N. Johnson, G. A. Mair, A. C. T. North, D. C. Phillips, and V. R. Sarma. 1967. *Proc. R. Soc. Ser. B Biol. Sci.* 167:378.

Blake, C. C. F., G. A. Mair, A. C. T. North, D. C. Phillips, and V. R. Sarma. 1967. On the conformation of the hen egg-white lysozyme molecule. *Proc. Roy. Soc. Ser. B. Biol. Sci.* 167:365–377.

Boué, F., F. Lefaucheux, M. C. Robert, and I. Rosenman. 1993. Small angle neutron scattering study of lysozyme solutions. *J. Cryst. Growth.* 133:246–254.

Bruzzesi, M. R., E. Chiancone, and E. Antonini. 1965. Association-dissociation properties of lysozyme. *Biochemistry.* 4:1796–1800.

Chiew, Y. C., D. E. Kuehner, H. W. Blanch, and J. M. Prausnitz. 1995. Molecular thermodynamics of salt-induced protein precipitation. *Am. Inst. Chem. Eng. J.* 41:2150–2159.

Clegg, S. L., S. Milioto, and D. A. Palmer. 1996. Osmotic and activity coefficients of aqueous $(NH_4)_2SO_4$ as a function of temperature, and aqueous $(NH_4)_2SO_4$-H_2SO_4 mixtures at 298.15 K and 323.15 K. *J. Chem. Eng. Data.* 41:455–467.

Coen, C. J., H. W. Blanch, and J. M. Prausnitz. 1995. Salting out of aqueous proteins: phase equilibria and intermolecular potentials. *Am. Inst. Chem. Eng. J.* 41:996–1004.

Corti, M., and V. Digiorgio. 1981. Quasi-elastic light scattering study of intermicellar interactions in aqueous sodium dodecyl sulfate solutions. *J. Phys. Chem.* 85:711–717.

Curtis, R. A., H. W. Blanch, and J. M. Prausnitz. 1997. Protein-protein and protein-salt interactions in aqueous protein solutions containing concentrated electrolyte. *Biotech. Bioeng.* (in press).

Deonier, R. C., and J. W. Williams. 1970. Self-association of muramidase (lysozyme) in solution at 25°C, pH 7.0, and I = 0.20. *Biochemistry.* 9:4260–4267.

Eberstein, W., Y. Georgalis, and W. Saenger. 1994. Molecular interactions in crystallizing lysozyme solutions studied by photon correlation spectroscopy. *J. Cryst. Growth.* 143:71–78.

Felderhof, B. U. 1978. Diffusion of interacting Brownian particles. *J. Phys. A Math. Gen.* 11:929–937.

George, A., and W. W. Wilson. 1994. Predicting protein crystallization from a dilute solution property. *Acta Crystallogr.* D50:361–365.

Hamaker, H. C. 1937. The London-van der Waals attraction between spherical particles. *Physica A.* 4:1058–1072.

Haynes, C. A., E. Sliwinsky, and W. Norde. 1994. Structural and electrostatic properties of globular proteins at a polystyrene-water interface. *J. Coll. Interf. Sci.* 164:394–409.

Horvath, A. L. 1985. Handbook of Aqueous Electrolyte Solutions: Physical Properties, Estimation and Correlation Methods. Ellis Horwood, Chichester, England.

Israelachvili, J. N. 1992. Intermolecular and Surface Forces, 2nd Ed. Academic Press, London.

Koppel, D. E. 1972. Analysis of macromolecular polydispersity in intensity correlation spectroscopy: the method of cumulants. *J. Chem. Phys.* 57:4814–4820.

Mahadevan, H., and C. K. Hall. 1992. Theory of precipitation of protein mixtures by nonionic polymer. *Am. Inst. Chem. Eng. J.* 38:573–591.

Melander, W., and C. Horvath. 1977. Salt effects on hydrophobic interactions in precipitation and chromatography of proteins: an interpretation of lyotropic series. *Arch. Biochem. Biophys.* 183:200–215.

Mikol, V., E. Hirsch, and R. Giegé. 1990. Diagnostic of precipitant for biomacromolecule crystallization by quasi-elastic light scattering. *J. Mol. Biol.* 213:187–195.

Murphy, R. M., M. L. Yarmush, and C. K. Colton. 1991. Determining molecular weight distribution of antigen-antibody complexes by quasi-elastic light scattering. *Biopolymers.* 31:1289–1295.

Muschol, M., and F. Rosenberger. 1995. Interactions in undersaturated and supersaturated lysozyme solutions: static and dynamic light scattering results. *J. Chem. Phys.* 103:10424–10432.

Muschol, M., and F. Rosenberger. 1996. Lack of evidence for prenucleation aggregate formation in lysozyme crystal growth solutions. *J. Cryst. Growth.* 167:738–747.

Nicoli, D. F., and G. B. Benedek. 1976. Study of thermal denaturation of lysozyme and other globular proteins by light-scattering spectroscopy. *Biopolymers.* 15:2421–2437.

Niimura, N., M. Ataka, Y. Minezaki, and T. Katsura. 1995. Small-angle neutron scattering from lysozyme crystallization process. *Physica B.* 213 and 214:745–747.

Norton, R. S., and A. Allerhand. 1977. Participation of tryptophan 62 in the self-association of hen egg white lysozyme. *J. Biol. Chem.* 252: 1795–1798.

Phillies, G. D. J. 1995. Dynamics of Brownian probes in the presence of mobile or static obstacles. *J. Phys. Chem.* 99:4265–4272.

Phillies, G. D. J., R. H. Hunt, K. Strang, and N. Sushkin. 1995. Aggregation number and hydrodynamic hydration levels of Brij-35 micelles from optical probe studies. *Langmuir.* 11:3408–3416.

Provencher, S. W. 1982a. A constrained regularization method for inverting data represented by linear algebraic or integral equations. *Comput. Phys. Commun.* 27:213–227.

Provencher, S. W. 1982b. CONTIN: a general purpose constrained regularization program for inverting noisy linear algebraic and integral equations. *Comput. Phys. Commun.* 27:229–242.

Pusey, P. N., and R. J. A. Tough. 1985. Particle interactions. *In* Dynamic Light Scattering: Applications of Photon Correlation Spectroscopy. R. Pecora, editor. Plenum Press, New York.

Riès-Kautt, M., and A. Ducruix. 1994. Crystallization of previously desalted lysozyme in the presence of sulfate ions. *Acta Crystallogr.* D50: 366–369.

Rosenbaum, D., P. C. Zamora, and C. F. Zukoski. 1996. Phase behavior of small attractive colloidal particles. *Phys. Rev. Lett.* 76:150–153.

Roth, C. M., B. L. Neal, and A. M. Lenhoff. 1996. Van der Waals interactions involving proteins. *Biophys. J.* 70:977–987.

Rothstein, F. 1994. Protein Purification Process Engineering. Dekker, New York.

Rupley, J. A., L. Butler, M. Gerring, F. J. Hartdegen, and R. Pecoraro. 1967. Studies on the enzymatic activity of lysozyme. III. The binding of saccharides. *Proc. Natl. Acad. Sci. USA.* 57:1088–1095.

Russel, W. B., D. A. Saville, and W. R. Schowalter. 1989. Colloidal Dispersions. Cambridge University Press, Cambridge.

Scopes, R. K. 1994. Protein Purification: Principles and Practice. Springer Verlag, New York.

Shen, C. L., G. L. Scott, F. Merchant, and R. M. Murphy. 1995. Light-scattering analysis of fibril growth from the amino-terminal fragment of β(1–28) of β-amyloid protein. *Biophys. J.* 65:2383–2395.

Skouri, M., M. Delsanti, J.-P. Munch, B. Lorber, and R. Giegé. 1991. Dynamic light scattering studies of the aggregation of lysozyme under crystallization conditions. *FEBS Lett.* 259:84–88.

Skouri, M., J.-P. Munch, B. Lorber, R. Giegé, and S. Candau. 1992. Interactions between lysozyme molecules under precrystallization conditions studied by light scattering. *J. Cryst. Growth.* 122:14–20.

Sophianopoulos, A. J. 1969. Association sites of lysozyme in solution. *J. Biol. Chem.* 244:3188–3193.

Sophianopoulos, A. J., C. K. Rhodes, D. N. Holcomb, and K. E. Van Holde. 1962. Physical studies of lysozyme. I. Characterization. *J. Biol. Chem.* 237:1107–1112.

Sophianopoulos, A. J., and K. E. Van Holde. 1961. Evidence for dimerization of lysozyme in alkaline solution. *J. Biol. Chem.* 236:PC82–PC83.

Sophianopoulos, A. J., and K. E. Van Holde. 1964. Physical studies of muramidase (lysozyme). II. pH-dependent dimerization. *J. Biol. Chem.* 239:2516–2524.

Stepanek, P. 1993. Data analysis in dynamic light scattering. *In* Dynamic Light Scattering: The Method and Some Applications. W. Brown, editor. Clarendon Press, Oxford.

Sushkin, N. V., and G. D. J. Phillies. 1995. Charged dielectric spheres in electrolyte solutions: induced dipole and counterion exclusion effects. *J. Chem. Phys.* 103:4600–4612.

Tanford, C., and M. L. Wagner. 1954. Hydrogen ion equilibria of lysozyme. *J. Am. Chem. Soc.* 76:3331–3336.

Tavares, F. W., and S. I. Sandler. 1997. Phase equilibrium for the mean-force potential of globular protein solutions. *Am. Inst. Chem. Eng. J.* 43:218–231.

Thibault, F., J. Langowski, and R. Leberman. 1992. Optimizing protein crystallization by aggregate size distribution analysis using dynamic light scattering. *J. Cryst. Growth.* 122:50–59.

Verwey, E. J. W., and J. T. G. Overbeek. 1948. Theory of Stability of Lyophobic Colloids. Elsevier, Amsterdam.

Vlachy, V., H. W. Blanch, and J. M. Prausnitz. 1993. Liquid-liquid phase separations in aqueous solutions of globular proteins. *Am. Inst. Chem. Eng. J.* 39:215–223.

Wang, F., J. Hayter, and L. J. Wilson. 1996. Salt-induced aggregation of lysozyme studied by cross-linking with glutaraldehyde: implications for crystal growth. *Acta Cryst.* D52:901–908.

Weast, R. C. 1981. Handbook of Chemistry and Physics, 62nd Ed. CRC Press, Boca Raton, FL.

Weiner, B. B. 1984. Particle sizing using photon correlation spectroscopy. *In* Modern Methods of Particle Size Analysis. H. Barth, editor. John Wiley and Sons, New York. 93–116.

Wills, P. R., L. W. Nichol, and R. J. Siezen. 1980. The indefinite self-association of lysozyme: consideration of composition-dependent activity coefficients. *Biophys. Chem.* 11:71–82.

Wilson, L. J., L. Adcock, and M. L. Pusey. 1993. A dialysis technique for determining aggregate concentrations in crystallizing protein solutions. *J. Cryst. Growth.* 122:8–13.

Wilson, L. J., L. Adcock-Downey, and M. L. Pusey. 1996. Monomer concentrations and dimerization constants in crystallizing lysozyme solutions by dialysis kinetics. *Biophys. J.* 71:2123–2129.

Zero, K., and R. Pecora. 1985 Dynamic depolarized light scattering. *In* Dynamic Light Scattering: Applications of Photon Correlation Spectroscopy. R. Pecora, editor. Plenum Press, New York.